Cryogenic performance of FOURIER, the initial science combiner at the MROI

Daniel J. Mortimer[a], David F. Buscher[a], Michelle J. Creech-Eakman[b], Chris Haniff[a], Christopher Salcido[b], Eugene Seneta[a], Xiaowei Sun[a], and John Young[a]

[a]Cambridge University, Cavendish Laboratory, JJ Thomson Ave, Cambridge, UK
[b]Magdalena Ridge Observatory/New Mexico Tech, 801 Leroy Place, Socorro, NM, USA

ABSTRACT

FOURIER is the first-generation science beam combiner for the MROI. It is a three-way, J, H and K band image plane combiner. The FOURIER design emphasises low visibility losses and high optical throughput and is designed around a low-noise SAPHIRA detector. Based on laboratory measurements of its throughput and visibility losses, FOURIER is expected to reach limiting magnitudes of 12.3, 13.2 and 11.7 in the J, H and K bands, respectively, within 5 minutes of incoherent integration assuming $0.7''$ seeing and a detector read noise of 0.3 electrons. As FOURIER observes as red as the K band, the detector and most of its optics are placed within a liquid nitrogen cryostat. We present the design of FOURIER's cryostat, as well as laboratory tests of the instrument's cryogenic performance. We also report room temperature characterisation of the optics. Finally, we discuss the path forward from the current status of the instrument to first fringes in 2023.

Keywords: Image plane beam combination, free space optics, faint limiting magnitudes, laboratory tests

1. INTRODUCTION

The Magdalena Ridge Observatory Interferometer (MROI) is a next generation long baseline optical interferometer (Buscher et al. 2013)[1] under construction in New Mexico, USA. Upon completion it will utilize a 10-telescope array with 28 Unit Telescope (UT) stations arranged in a equilateral Y shape operating on baselines between 7.8–347 metres, and will conduct observations in both the visible and near-infrared (λ=0.6 µm–2.4 µm). The project is currently progressing towards operating three telescopes. Work is currently preparing for the arrival of the second telescope ahead of first fringes in Q2 of 2023.

The Free-space Optical multi-apertUre combineR for IntERferometry (FOURIER) is undergoing final tests at the University of Cambridge and will be the first generation science combiner. FOURIER is a three-way, spectrally dispersed and cryogenically cooled image plane combiner and will operate in the J, H and K bands (λ = 1.1 µm–2.4 µm). It will perform the first closure phase measurements at the array, conduct early science as well as assist in demonstrating the baseline bootstrapping capabilities of the MROI (Creech-Eakman et al. 2018).[2]

In this proceeding we provide an update on the development of FOURIER since the last SPIE meeting. The warm laboratory tests of the optics have now been completed and the instrument has been shown to meet the expected levels of performance against all metrics tested: beam shaping, throughput, instrumental visibility and spectral resolution. Here we present measurements of the throughput and refined measurements of the spectral resolution. Performance of the instrument as measured using the other metrics has been presented in our previous proceeding (Mortimer et al. 2020).[3]

In addition to the warm laboratory tests, the instrument has now been integrated into its cryostat and is routinely operated at Liquid Nitrogen (LN2) temperatures. Here we present the design of the cryostat as well as preliminary cryogenic results from the instrument.

Further author information: Send correspondence to D.J.M
E-mail: d.j.mortimer@exeter.ac.uk,

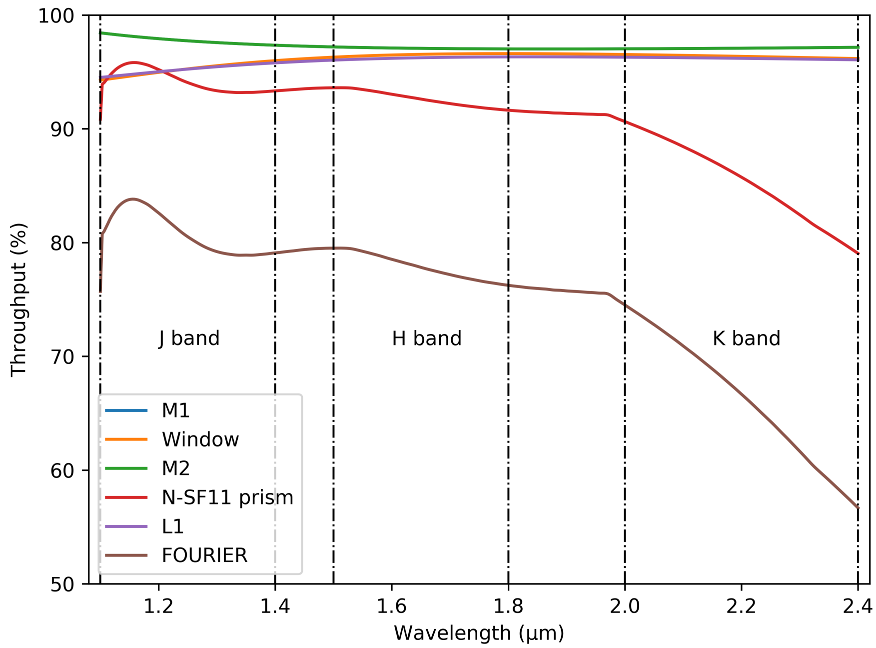

Figure 1. The theoretical optical throughput of FOURIER modelled by Zemax. This is with the exception of the multi-layer anti-reflection coating on the N-SF11 prism which was not modelled in Zemax but instead by theoretical throughput curves provided by Thin Films Inc. The theoretical throughput achieved is 80.5%, 78% and 66.5% at the centres of the J, H and K bands respectively. The noticeable drop off in the K band being due to internal absorption by the N-SF11 glass.

2. WARM LABORATORY TESTS

The room temperature laboratory tests to validate the optical design of FOURIER have now been completed. Here we present the results of two tests, a measurement of the throughput and of the spectral resolution of the instrument. We refer the reader to our earlier proceeding paper for a summary of the optical layout of FOURIER and of our warm laboratory tests setup (Mortimer et al. 2020).[3]

2.1 Throughput

As FOURIER is designed to be a high sensitivity combiner, reaching a high throughput is a top priority and a large motivation for the bulk optics design of FOURIER.

Figure 1 shows the theoretical throughput for the optical components of FOURIER. The throughput for each optical surface was calculated using the reflection vs wavelength tool in Zemax. The internal transmission loss was calculated by the internal transmission tool. This is with the exception of the anti-reflection coating applied to the N-SF11 dispersing prism. For this element the theoretical throughput curves were provided by Thin Films Inc for a custom multi-layer anti-reflection coating designed for FOURIER. The theoretical throughput achieved is 80.5%, 78% and 66.5% at the centres of the J, H and K bands respectively. The noticeable drop off in the K band is due to internal absorption by the N-SF11 glass. This is compared to a typical throughput of around 65% for integrated optics beam combination chips (Benisty et al. 2009).[4]

The goal of this work was to confirm this throughput by measuring it in the laboratory. We achieved this by launching two beams from a thermal white light source through FOURIER and measuring the flux from each beam before and after the FOURIER combiner optics. To measure the flux before the FOURIER optics we placed a Raptor Owl 640M camera at the focal plane of M1, measuring the detector counts through a series of narrowband near-infrared filters. We repeated the measurement at the SAPHIRA detector focal plane, after the FOURIER combiner optics. We processed the frames by applying dark frames, bias frames and flat frames. To estimate the extent of the Point Spread Function (psf) we studied the encircled energy around the psf produced

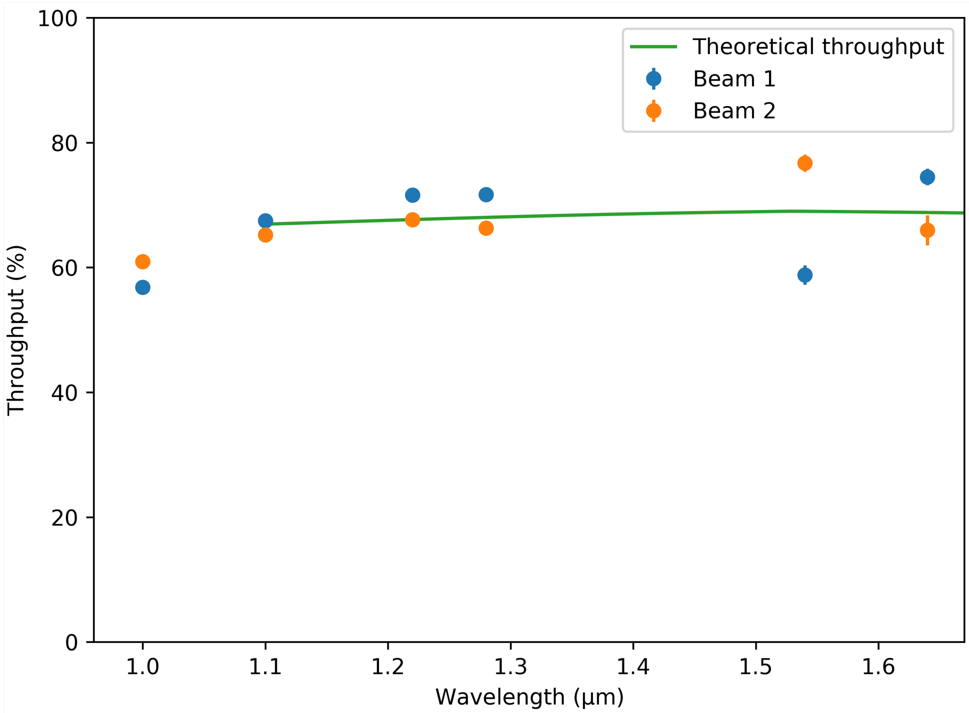

Figure 2. The measured laboratory throughput of the FOURIER combiner optics (cryostat window, M2, N-SF11 prism and L1) for two white light source beams (beam 1 and beam 2) plotted alongside the throughput calculated from the Zemax models of FOURIER.

at each focal plane to define a flux counting box and ensure we do not cut off any of the light from the light source.

With these corrections we estimated the throughput by taking the ratio of the sum of detector counts within our flux counting boxes through each filter and for each beam. The result of these measurements is shown in figure 2.

The error bars in figure 2 are estimated by dividing the series of light frames recorded into an number of equally sized bins, and calculating the standard deviation of the mean values from each of those bins to compute the standard error of the mean. The error bars are typically smaller than the scatter points except for the $\lambda = 1.64\,\mu\text{m}$ filter.

The measurements agree well with the theoretical throughput. Here beam 1 and beam 2 represent the two beams of our laboratory light source. The expected theoretical throughput from the Zemax model is the green solid line. The difference between the measured and theoretical throughput is on average only 3.8%, with the greatest difference being 10.2% in the $\lambda = 1.54\,\mu\text{m}$ filter. This calculation includes the throughput of all but one of the FOURIER combiner optics, it includes the cryostat window, M2, the N-SF11 prism and L1. The measured and theoretical throughput shown in figure 2 is around 15% lower than the estimated throughput shown in figure 1 as the N-SF11 prism was uncoated during these tests. The prism will be coated before the instrument is delivered to the MROI.

2.2 Spectral resolution

The light in FOURIER is spectrally dispersed by a N-SF11 equilateral prism. To validate the prisms dispersive properties we implemented a Fourier Transform Spectrometer (FTS) mode of our laboratory white light source to enable us to extract a spectrum for each spectral channel of FOURIER. With this we could measure the spectral resolution and perform wavelength calibration of the instrument.

We presented preliminary results and a explanation of the methodology in our last contribution (Mortimer et al. 2020)[3] however we will also summarise the technique here. We used the two white light beams from

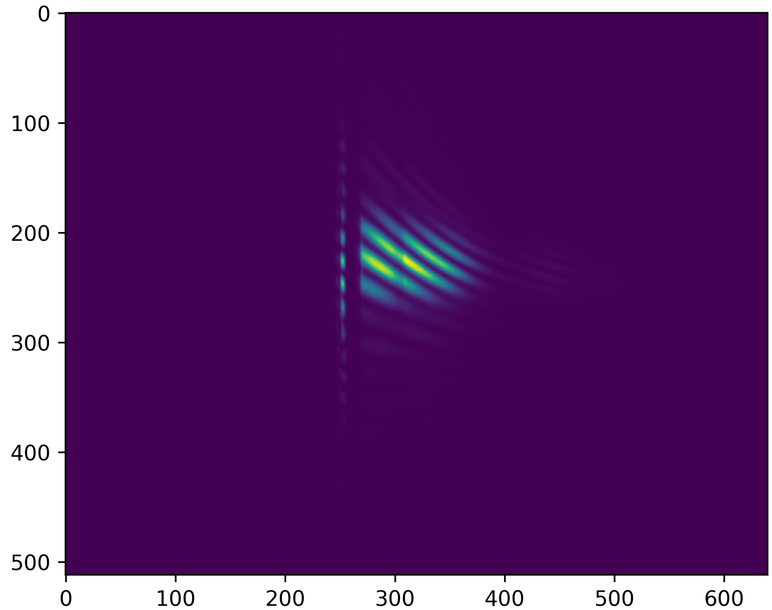

Figure 3. A single frame from our FTS measurements. The narrow modulated spectrum to the left of the frame is from the $\lambda = 1.31\,\mu$m laser used to calibrate the step size of the Agilis linear stage. To the right of this is the spectrally dispersed white light fringe pattern.

our laboratory light source to produce interference fringes on the detector. We placed an Agilis AG-LS25-27 linear stage under a periscope in one of the beams to allow us to modulate its path length. By monitoring the modulation of the interference fringes for a fixed pixel using a reference laser of known wavelength (Thorlabs S3FC1310, $\lambda = 1.31\,\mu$m), offset at a slight angle from the white light source to not overlap on the detector, we were able to monitor the distance the Agilis linear stage moved with each step. An example frame of the laser and white light source is shown in figure 3 where the horizontal axis is the spectral direction and the vertical axis shows the interference fringes.

With the calibrated step size we were able to scan through the coherence envelope and produce the data shown in figure 4 where the detector count for a single pixel is plotted against the Optical Path Difference (OPD) as the Agilis modulates the path length. The average step size of the Agilis was 270 nm, providing 3.7 measurements per fringe cycle at the shortest wavelengths so our interferogram is well sampled. By measuring the intensity vs OPD in each row of pixels along the spectral axis and taking the Fourier transform of this data we were able to produce a spectra for each row of pixels which shows a Gaussian like peak centred on the central wavelength in that channel. By fitting a Gaussian function to the recovered spectrum we calculate the spectral resolution $R = \lambda/\Delta\lambda$ by taking λ to be the mean of the fitted Gaussian and $\Delta\lambda$ the full width half maximum of the Gaussian.

From this data we plotted the spectral resolution as a function of wavelength as shown in figure 5. The spectral resolution is consistent with the values predicted from the design of FOURIER. For example at the centre of the J band ($\lambda = 1.25\,\mu$m) the simulated R value was 89 and is calculated here to be 97. For the H band ($\lambda = 1.65\,\mu$m) the simulated value was 75 and here was measured to be 83. The artefact centred around $\lambda = 1.38\,\mu$m is caused by the light source which has a rapid change in intensity as a function of wavelength in this region and skews the Gaussian fit to the spectra giving rapidly changing R values. The $\lambda = 1.68\,\mu$m artefact is caused by the detector quantum efficiency which drops rapidly at this wavelength, suppressing the longer wavelengths of light in each spectral channel, reducing the FWHM of the fitted Gaussian and hence increasing the R value extracted. This effect disappears when the quantum efficiency stabilises again at around $\lambda = 1.7\,\mu$m.

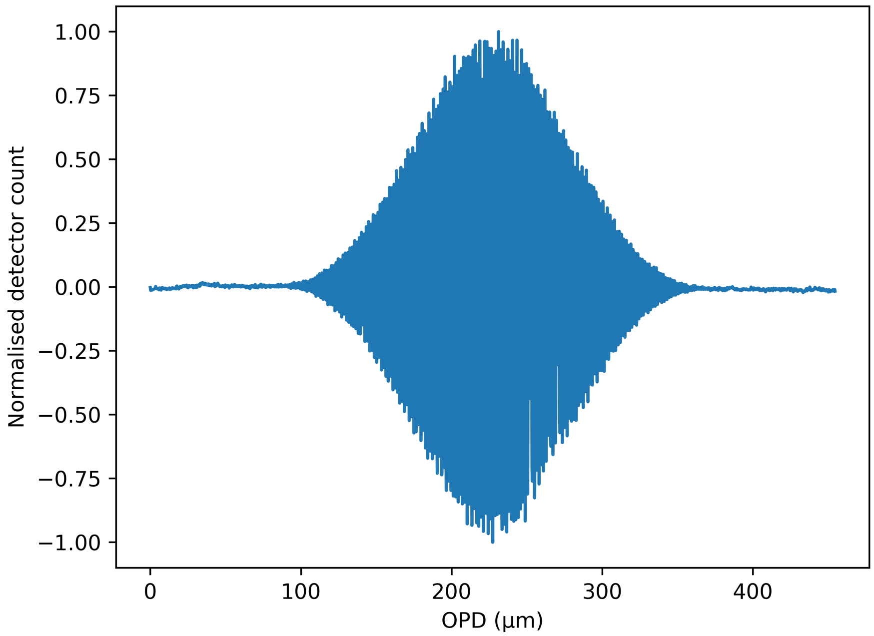

Figure 4. The coherence envelope for one spectral channel measured by recording the intensity of a single pixel as the Agilis linear stage modulates the path length difference between the two coherent white light beams in our laboratory light source.

These spectral resolution values are significantly higher than the R = 63 and R = 53 in the J and H bands respectively presented in our previous proceedings (Mortimer et al. 2020).[3] The lower spectral resolution in our previous work was found to be due to a defocus along the spectral axis of the instrument.

Finally, we plotted the central wavelength for each row of pixels along the spectral axis vs distance along the detector (assuming a pixel pitch of 15 µm for the Raptor Owl 640M) and compared it to the dispersion predicted from the Zemax model. The dispersion was extracted from Zemax by measuring the centroid of the spot diagram for a series of wavelengths, automating the process with PYZDDE (Sinharoy et al. 2015).[5] The comparison of the measured and modelled data is shown in figure 6 where the two show good agreement with a slight slope in the residual between the data and model. This linear slope in the residuals is likely due to a tilt error of the detector with respect to the incoming beams in the laboratory setup.

3. CRYOSTAT DESIGN

As FOURIER operates as red as the K band in the near-infrared the detector is sensitive to thermal photons from room temperature objects. This, combined with the fact that the SAPHIRA detector requires temperatures of 80K to operate effectively (Lanthermann et al. 2019)[6] means FOURIER requires some form of cryogenics for the detector. To minimise the thermal background further we placed most of the optics of the FOURIER combiner within the a cryogenic environment as well.

To meet this design requirement we procured a custom liquid nitrogen cryostat from Universal Cryogenics. A labelled diagram of the cryostat is show in figure 7 where the cryostat door and radiation shield lids have been removed for clarity.

All components within the cryostat are suspended from the roof, at the top of the suspended assembly is an 11L LN2 tank which can be filled and vented via the two ports labelled LN2 refill and LN2 vent at the top of the cryostat. Underneath the LN2 tank is the cold space envelope which houses the detector and cryogenic optics. The horizontal and vertical cold plate (to which the detector and all the optics are mounted) are cooled by

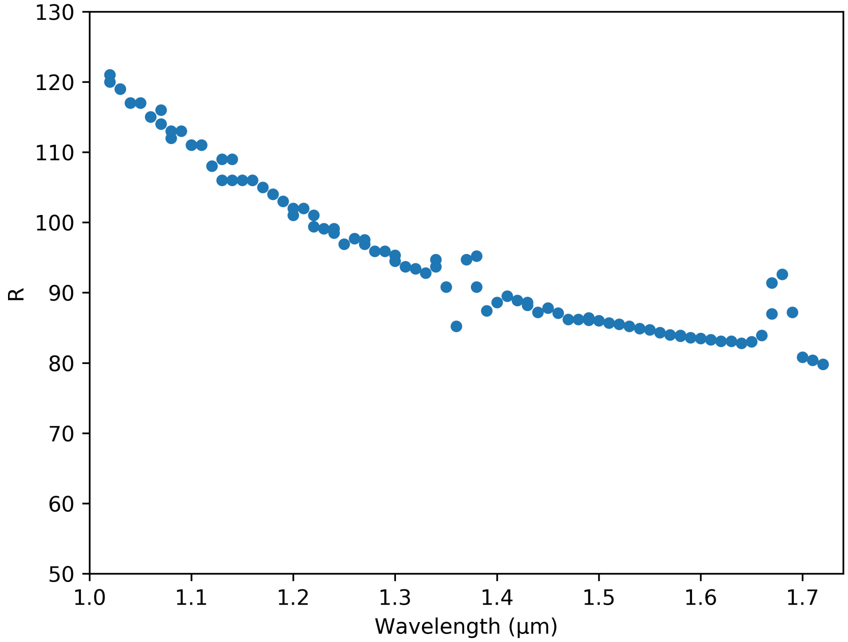

Figure 5. The spectral resolution calculated from the spectra extracted for each row along the spectral axis plotted against the central wavelength in each spectra. the spectral resolution values agree well with the values predicted from the design of FOURIER as described in the text. The artefacts centred around at $\lambda = 1.38\,\mu\text{m}$ and $\lambda = 1.68\,\mu\text{m}$ are known to be caused by the light source and detector quantum efficiency respectively as described in the text.

their thermal connection to the LN2 tank. The inner radiation shield is connected directly to the LN2 tank and encloses the cold space envelope, this shield is surrounded by the outer radiation shield which also covers the LN2 tank to shield them from the thermal photons from the room temperature outer casing of the cryostat. Finally, slots are placed in the radiation shields to pass through the cabling for the SAPHIRA detector, temperature sensors and heaters placed within the cryostat. These are wired to vacuum sealed connectors that are seated in the cable interface plate, from which room temperature cabling can be run to control the electronics within the cryostat.

An image of the cryostat in the laboratory in Cambridge is shown in figure 8. The beam path through the cold optics after entering the cryostat from the lower left corner of the image is drawn on in red. Also visible is the copper cold finger (top left) which thermally connects the detector to the LN2 tank to ensure the most efficient cooling.

4. COLD TESTS

We now routinely operate the FOURIER combiner within its cryostat and have begun validating the performance both of the cryostat and the instrument at cryogenic temperatures. In this section we present preliminary results from the cryogenic testing.

4.1 Temperature and hold time

One design requirement was to be able to operate the SAPHIRA detector at around 80K. Given the boiling temperature of liquid nitrogen of 77K a good thermal connection is needed between the LN2 tank and the detector which must be validated in laboratory testing. A second requirement placed on the cryostat was that the LN2 tank must not need to be refilled more than once per day (a hold time of at least 24 hours).

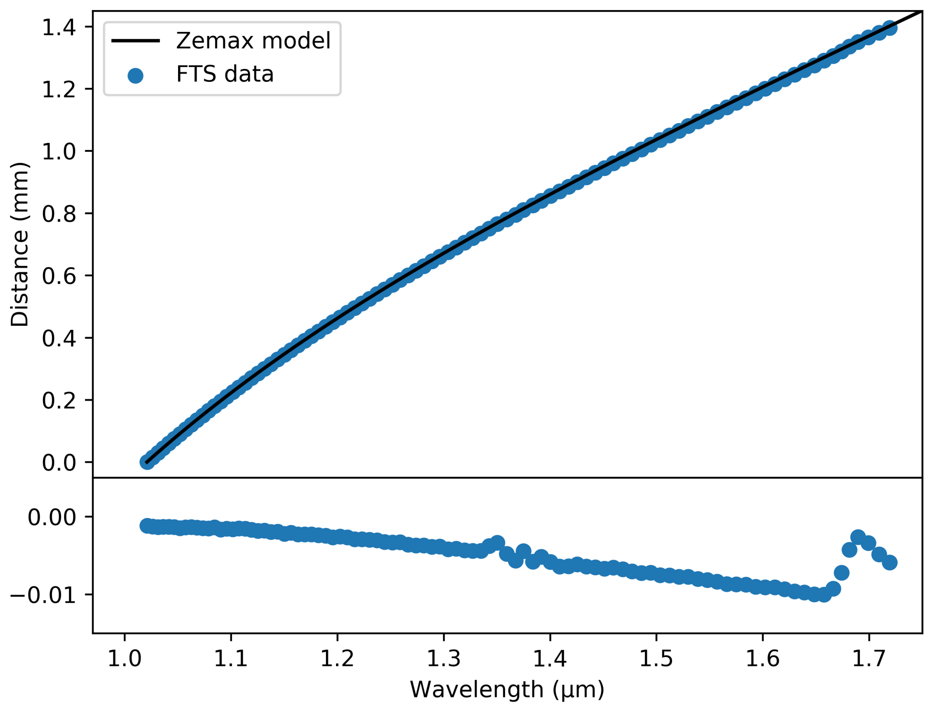

Figure 6. The central wavelength from the FTS spectra measured in each row of pixels along the spectral axis plotted against the distance along the detector. The measured dispersion is shown to match up well with the dispersion modelled in Zemax (the Zemax model line). Note the curved slope showing the dispersion decreasing towards longer wavelengths which is reflected in the lower R value at longer wavelengths in figure 5. The artefacts in the residuals centred around at $\lambda = 1.38\,\mu\text{m}$ and $\lambda = 1.68\,\mu\text{m}$ are due to the same reasons as the artefacts in figure 5 and are described in the text.

To measure the temperature performance of the cryostat we placed four temperature sensors around the cold space envelope. The first one is integrated into the SAPHIRA detector chip die (labelled detector) the second is placed on the cold finger connecting the detector to the LN2 tank (detector cold finger), a third is placed on the horizontal cold plate (horizontal cold plate) and a final fourth one is placed near the bottom of the vertical cold plate (vertical cold plate). To measure the temperature and hold time achieved we cooled the cryostat down to its operating temperature, refilled the LN2 tank and logged the temperature from the four sensors using a Lakeshore 336 temperature controller. The result of this test is shown in figure 9.

We were able to achieve a hold time of over 30 hours on a single tank and reach temperatures of 79K, very close to the boiling point of the liquid nitrogen. In addition, the temperature is very stable, for example the detector sensors measured temperature was 84.5 $\pm$ 0.03 K for the data shown in figure 9. This is achieved without any active control of the temperature. In the future we plan to temperature control the detector with a small heater placed on the cold finger to improve the stability further. The offset between the detector and other temperature sensors seen in figure 9 is believed to be a sensor calibration error and not a physical difference in temperature.

4.2 Fringe contrast

The ability of the FOURIER combiner to produce high contrast interference fringes was demonstrated in Mortimer et al. (2020)[3] however such high contrast fringes also need to be demonstrated after cooling down the instrument to cryogenic temperatures.

To reduce cost and complexity of the instrument there are no cryogenic motors within the FOURIER cryostat. The optical design of FOURIER utilises very slow beams of f/92 which give loose alignment tolerances of order

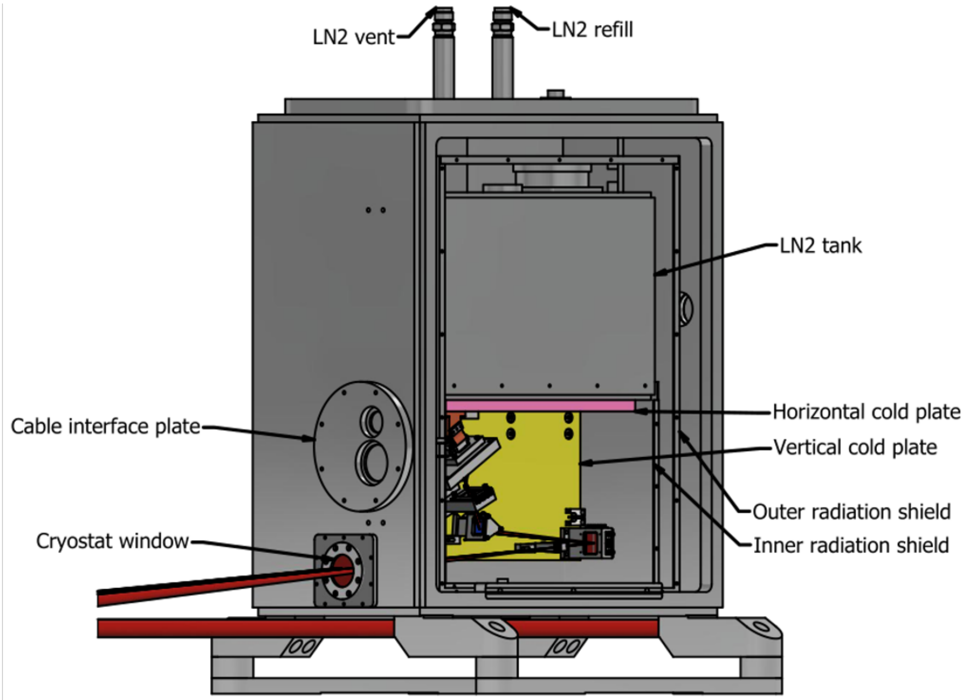

Figure 7. A labelled diagram of the FOURIER cryostat. The main assembly is suspended from the roof of the cryostat. At the top is an 11L LN2 tank underneath which is the cold space envelope which contains the detector and cryogenic optics. An image of this space during laboratory testing is shown in figure 8. This space is enclosed by the inner radiation shield which is connected directly to the LN2 tank. The outer radiation shield encloses both the inner radiation shield and the LN2 tank to stop thermal photons from the warm outer walls of the cryostat reaching these cold surfaces.

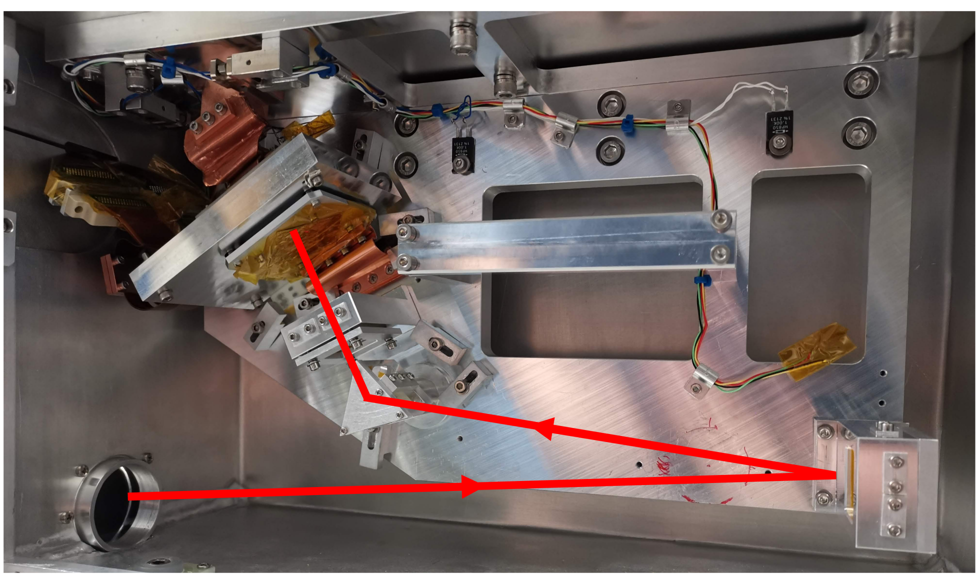

Figure 8. The optics and detector mounted in the cold space envelope of the FOURIER combiner cryostat. The beam path after the light enters the cryostat is shown in red. The light travels from the lower left of the image to M2 in the lower right where it is reflected and passes through the N-SF11 prism and L1 before coming to a focus on the SAPHIRA detector mounted in the top left of the image.

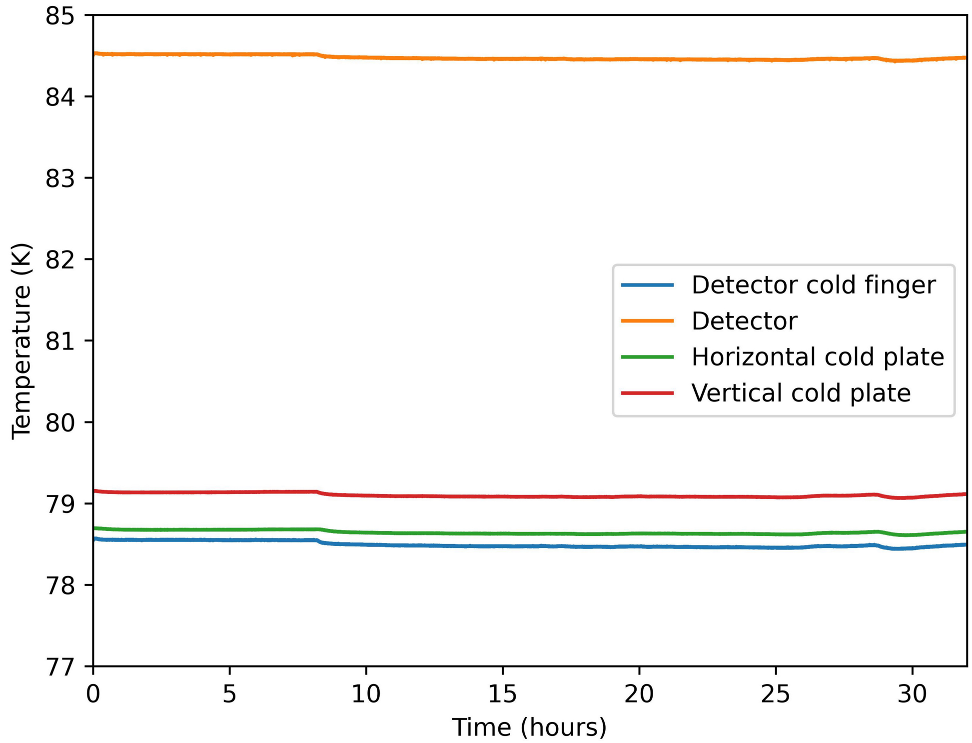

Figure 9. The temperature measured by the four sensors placed within the cold space envelope measured for one fill of the LN2 tank. The entire cold space envelope reached temperatures of around 79K for over 30 hours, exceeding both the temperature and hold time requirements.

hundreds of microns for the cryogenic optics (Mortimer. 2021).[7] After studying the expected movement of the optics due to thermal contraction as the instrument cools we concluded cryogenic motors were not necessary.

To demonstrate this in the laboratory we input two white light beams placed at the largest planned separation to produce the highest spatial frequency interference fringes and recorded the dispersed white light on the SAPHIRA detector as shown in figure 10. The highest fringe contrast in figure 10 gives a instrumental visibility 80%, this is compared to the fringe contrast of 84% measured for the same fringe frequency during the warm laboratory tests. This shows that the instrument still maintains good alignment after cooldown from room temperature to cryogenic temperatures. Future tests will attempt to improve the fringe contrast further by optimising the alignment of the cold optics as well as remeasuring the spectral resolution of the instrument when cold via the method described in section 2.2 as the warm tests showed the spectral resolution to be sensitive to defocus.

One thing to note is that the cold interference fringes were produced with beams only 5 mm in diameter as opposed to the 13 mm used during the warm tests and planned at the MROI observatory. This is due to vignetting of larger beams through our laboratory light source in its current configuration. The laboratory light source will be realigned and fringe contrast remeasured though we do not expect a change in the beam diameter to significantly affect the measured fringe contrast.

4.3 Thermal background

One of the main purposes of the FOURIER cryostat is to minimise the thermal background from room temperature objects. Cooling both the detector and optics and placing them in the same cold envelope also allows us to significantly cut down on the background.

To measure the thermal background we cooled the instrument to its operational temperature and recorded a series of 1,000 frames from the SAPHIRA detector with the instrument in its operational state such that thermal background light could enter the cryostat as it will during observations. Immediately after we then placed a

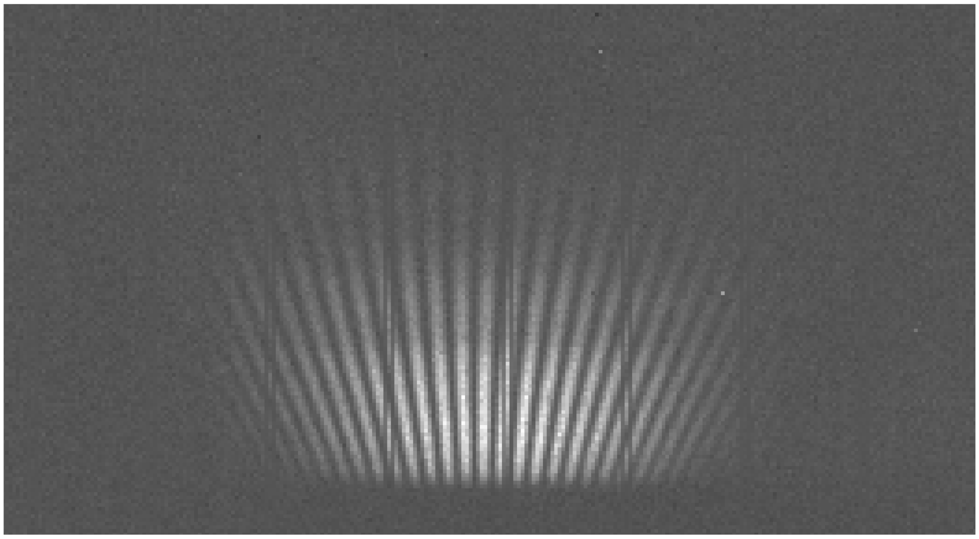

Figure 10. Dispersed white light fringes recorded on the SAPHIRA detector with the instrument at cryogenic temperatures. An instrumental visibility of 80% is measured in this frame. The vertical dark lines are detector artefacts arising from a loose connector, this has already been addressed.

flat mirror up against the cryostat entrance window to make the system as light tight as possible and minimize thermal photons entering the cryostat. We then recorded another 1,000 frames. By comparing the number of detector counts when the mirror is and isn't present we estimated the thermal background. For the tests shown here the gain was set to 1.8 e-/ADU. To process the data we found the mean counts of the 1,000 frames for each pixel in both data sets and subtracted the two to give us an estimate of the number of thermal photons per pixel. We then plotted a histogram for the thermal background of all pixels which is shown in figure 11. The exposure time of each individual frame was set to 2 ms however the thermal background for the data in figure 11 was multiplied up to estimate the thermal background for a 37 ms exposure (assuming the number of thermal photons increases linearly with exposure time) to better estimate the thermal background we would measure during a typical exposure at the MROI.

As figure 11 shows the thermal background is very high with a mean of 6,832 e-/pixel/exposure and must be addressed. This is likely due to the fact that we have not yet fitted cold stop or thermal baffling into the cryostat and we believe that stray thermal light is entering through the 2" cryostat window before reflecting off the interior of the radiation shield and reaching the detector.

To address this we will install a series of baffles culminating in a cold stop within the cold space envelope. There is plenty of space after the cryostat window in the lower left corner of the cold space envelope as figure 8 shows. Due to the slow f/92 beams beams used in FOURIER the cold stop is very small, of order a couple of mm in diameter. We therefore expect a significant improvement in the thermal background once the aperture through which stray thermal light can enter the cryostat is reduced from 2" to a few mm. Once the cold stop is installed we estimate that in the best case scenario the thermal photon count will be 0.04 e-/pixel/exposure at the centre of the K band.

5. FUTURE WORK

The warm laboratory tests have concluded and the instrument has met all its design requirements. We have subsequently installed the instrument in its cryostat. The cryostat is demonstrating a good hold time and excellent thermal performance (holding temperatures of 79K for over 30 hours on a single fill). We have begun to validate the system performance when cold, having demonstrated high contrast interference fringes and quantified the thermal background.

The next steps will be to continue validating the optical alignment of the system when cold, specifically by repeating the spectral resolution tests and attempting to maximise the fringe contrast further. In addition to

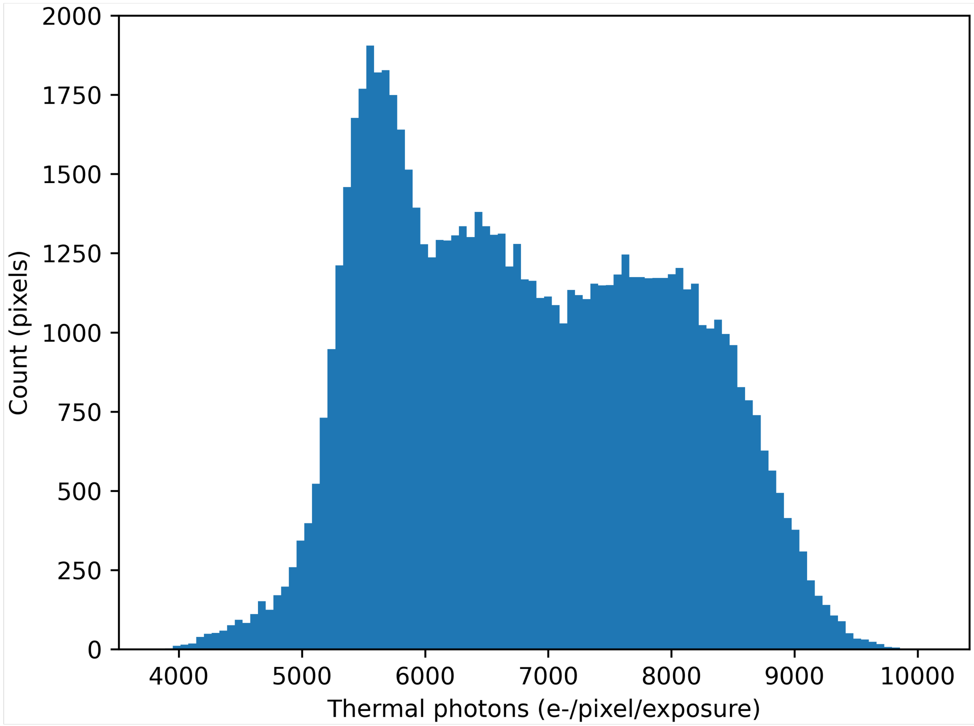

Figure 11. A histogram of the number of thermal photons per pixel measured by the method described in the text. The thermal background is very high with a mean of 6,832 e-/pixel/exposure. This is likely due to the fact that we have not yet fitted thermal baffling or a cold stop to the instrument and so thermal light enters the 2" window, reflecting off the radiation shields and onto the detector. Thermal baffling and a cold stop will be added and this test repeated before deployment at the MROI.

this the current thermal background will be addressed by adding a series of baffles and a cold stop. Once the cold tests are complete we will deliver FOURIER to the MROI where we will carry out a series of site acceptance tests ahead of first fringes in Q2 of 2023.

ACKNOWLEDGMENTS

This material is based on research sponsored by Air Force Research Laboratory (AFRL) under agreement number FA9453-22-2-0040. The U.S. Government is authorized to reproduce and distribute reprints for Governmental purposes notwithstanding any copyright notation thereon.

REFERENCES

[1] Buscher, D. F., Creech-Eakman, M., Farris, A., Haniff, C. A., and Young, J. S., "The Conceptual Design of the Magdalena Ridge Observatory Interferometer," *Journal of Astronomical Instrumentation* **2**, 1340001 (Dec. 2013).

[2] Creech-Eakman, M. J., Romero, V. D., Payne, I., Haniff, C. A., Buscher, D. F., Young, J. S., Santoro, F., Blasi, R., Dahl, C., Dooley, J., Etscorn, D., Farris, A., Fisher, M., Garcia, E., Gino, C., Jaynes, B., Jencka, L., Johnston, P., Jurgenson, C., Kelly, R., Klinglesmith, D., Ligon, E. R., Luis, J., McCracken, T. M., McKeen, C., Mortimer, D., Ochoa, D., Olivares, A., Pino, J., Salcido, C., Schmidt, L. M., Seneta, E. B., Sun, X., and Wilson, D., "The Magdalena Ridge Observatory interferometer: first light and deployment of the first telescope on the array," in [*Optical and Infrared Interferometry and Imaging VI*], Creech-Eakman, M. J., Tuthill, P. G., and Mérand, A., eds., *Society of Photo-Optical Instrumentation Engineers (SPIE) Conference Series* **10701**, 1070106 (July 2018).

[3] Mortimer, D. J., Buscher, D. F., Creech-Eakman, M. J., Haniff, C., Ligon, E., Luis, J., Salcido, C., Seneta, E., Sun, X., and Young, J., "First laboratory results from FOURIER, the initial science combiner at the MROI," in [*Society of Photo-Optical Instrumentation Engineers (SPIE) Conference Series*], *Society of Photo-Optical Instrumentation Engineers (SPIE) Conference Series* **11446**, 114460V (Dec. 2020).

[4] Benisty, M., Berger, J. P., Jocou, L., Labeye, P., Malbet, F., Perraut, K., and Kern, P., "An integrated optics beam combiner for the second generation VLTI instruments," *Astronomy & Astrophysics* **498**, 601–613 (May 2009).

[5] Sinharoy, I., xy124, Holloway, C., ng110, and Nummela, V., "Pyzdde: v1.0-alpha," (Mar. 2015).

[6] Lanthermann, C., Anugu, N., Le Bouquin, J. B., Monnier, J. D., Kraus, S., and Perraut, K., "Modeling the e-APD SAPHIRA/C-RED ONE camera at low flux level. An attempt to count photons in the near-infrared with the MIRC-X interferometric combiner," *Astronomy & Astrophysics* **625**, A38 (May 2019).

[7] Mortimer, D., *Designing a beam combiner for faint limiting magnitudes in optical interferometry*, PhD thesis, University of Cambridge (2021).